journal of the mechanical behavior of biomedical materials 118 (2021) 104397

Contents lists available at ScienceDirect

Journal of the Mechanical Behavior of Biomedical Materials

journal homepage: http://www.elsevier.com/locate/jmbbm

Damage in extrusion additive manufactured biomedical polymer: Effects of testing direction and environment during cyclic loading

Amirpasha Moetazedian [a], Andrew Gleadall [a,*], Elisa Mele [b], Vadim V. Silberschmidt [a]

[a] Wolfson School of Mechanical, Electrical and Manufacturing Engineering, Loughborough University, Loughborough, LE11 3TU, UK
[b] Department of Materials, Loughborough University, Loughborough, LE11 3TU, UK

ARTICLE INFO

Keywords:
Additive manufacturing
Polylactide
Damage
Interface
Submerged

ABSTRACT

Although biodegradable polymers were widely researched, this is the first study considering the effect of combined testing environments and cyclic loading on the most important aspect related to additive manufacturing: the interfacial bond between deposited layers. Its results give confidence in applicability of the material extrusion additive manufacturing technology for biomedical fields, by demonstrating that the interface behaves in a manner similar to that of the bulk-polymer material. To do this, especially designed tensile specimens were used to analyse the degradation of 3D-printed polymers subjected to constant-amplitude and incremental cyclic loads when tested in air at room temperature (control) and submerged at 37 °C (close to in-vivo conditions). The mechanical properties of the interface between extruded filaments were compared against the bulk material, i.e. along filaments. In both cases, cyclic loading caused only a negligible detrimental effect compared to non-cyclic loading (less than 10 % difference in ultimate tensile strength), demonstrating the suitability of using 3D-printed components in biomedical applications, usually exposed to cyclic loading. For cyclic tests with a constant loading amplitude, larger residual deformation (>100 % greater) and energy dissipation (>15 % greater) were found when testing submerged in solution at 37 °C as opposed to in laboratory conditions (air at room temperature), as used by many studies. This difference may be due to plasticisation effects of water and temperature. For cyclic tests with incrementally increasing loading amplitudes, the vast majority of energy dissipation happened in the last two cycles prior to failure, when the polymer approached the yield point. The results demonstrate the importance of using an appropriate methodology for biomedical applications; otherwise, mechanical properties may be overestimated.

1. Introduction

Synthetic bioresorbable polymers are broadly utilised in several sectors, including biomedical applications, due to their potential for more tailored mechanical (i.e. strength, modulus and strain at failure) and chemical properties (i.e. molecular weight) compared to natural polymers (Nair and Laurencin, 2007), (Da Silvaet al., 2018). Polylactide (PLA) is one of the most studied polymers, which can be produced by fermentation of sugarcane (Da Silvaet al., 2018). Its good processability along with higher strength and stiffness and, importantly, excellent biocompatibility compared to other synthetic polymers, make it an excellent candidate for biomedical applications (Farah et al., 2016), (Elsawy et al., 2017). These range from orthopaedic screws and fixation plates to scaffolds for tissue engineering and drug-delivery devices (Da Silvaet al., 2018), (Farah et al., 2016), (Xu et al., 2016), (Gleadall et al., 2018a).

In recent decades, additive manufacturing (AM) has revolutionised the manufacturing industry and attracted significant interest from various sectors (Ligon et al., 2017). One of the key driving forces for the rapid development of the AM industry is the capability to fabricate customised, complex and intricate components, which otherwise cannot be achieved with conventional subtractive manufacturing processes (Gleadall et al., 2018a), (Gleadall et al., 2018b), (Bachtiaret al., 2020). Material extrusion additive manufacturing (MEAM) - also known as *fused filament fabrication (FFF)* and *fused deposition modelling (FDM)* - is the most commonly used AM technology for many thermoplastic polymers including PLA. In this method a molten polymer is extruded through a heated nozzle onto a print platform. After prescribed movements of the nozzle parallel to the print platform (X–Y direction) to deposit arrays of extruded filaments for one layer, the print platform

* Corresponding author.
E-mail address: A.Gleadall@lboro.ac.uk (A. Gleadall).

https://doi.org/10.1016/j.jmbbm.2021.104397
Received 30 October 2020; Received in revised form 2 February 2021; Accepted 11 February 2021
Available online 20 February 2021

moves down incrementally (Z direction) to create the part layer by layer. One of the main limitations in MEAM parts reported in the literature is poor bonding between extruded filaments, especially in the Z direction. Studies investigated the effect of different printing parameters on the interface strength of 3D-printed parts using a range of adapted polymer-testing standards "Coogan and Kazmer 2017, Spoerk et al 2018, Aliheidari et al 2018, Bellehumeur and Li, 2004, Pan et al 2015 and Spoerk et al 2017. However, results are often contradicting, with some studies (Ning et al., 2017), (Christiyan et al., 2016), (Abbott et al., 2018) reporting enhanced strength at lower printing speeds, and others (Coogan and Kazmer, 2017a), (Pan et al., 2015), (Coogan and Kazmer, 2017b) reporting the opposite trend. The contradictions are most likely due to the complexity and variability of testing design, which prevents accurate measurement of samples' microscale geometry for strength analysis (Allum et al., 2020).

PLA is susceptible to changes in the surrounding environment including moisture, temperature and loading conditions (Moetazedian et al., 2020a). From a biomedical perspective, a 3D-printed PLA implant should tolerate both mechanical and environmental stresses that may take place during its in-service use (Lawrence et al., 2001), (Wu et al., 2006). In particular, polymeric implants are likely to be subjected to sub-critical repetitive loading/unloading conditions (Safai et al., 2019). Such conditions may result in damage accumulation, which ultimately causes failure of implants earlier than expected. Previous studies (Senatov et al., 2016), (Gong et al., 2017), (Afrose et al., 2016) considered the fatigue life of 3D-printed PLA parts under compression and tension. Only the study by Afrose et al. (2016) considered the fatigue life of 3D-printed PLA with respect to the interfacial bond (Z-direction), with anisotropic properties identified, although the actual contact area was not considered for bond-strength calculations, which is a critical factor (Allum et al., 2020). Therefore, there is a lack of understanding of the damage evolution for the most critical aspect related to AM: the interfacial bond between layers. Furthermore, previous studies (Senatov et al., 2016)– (Afrose et al., 2016) only considered cyclic loading conditions for specimens tested in air. Meanwhile, in our previous study (Moetazedian et al., 2020a), the importance of the testing environment for the correct assessment of 3D-printed PLA was demonstrated. It showed that testing PLA submerged in water at physiological temperature (PT, 37 °C) instead of in air at room temperature (RT) avoids a potential two-fold overestimation of mechanical properties. The current study investigates for the first time, the damage evolution for bulk material and interfaces between 3D-printed layers under medically relevant conditions to identify sensitivity of properties to testing environment for constant-amplitude and incremental-amplitude cyclic loading conditions.

2. Materials and methods

2.1. Specimen design and additive manufacturing

Natural polylactide (PLA) filament (3DXTECH® branded NatureWorks® polylactide 4043D, Sigma Aldrich) was used to produce four walls comprised of single filaments in the form of square with dimensions of 45 mm × 45 mm and height of 45 mm (Fig. 1a) using a RepRap ×400 MEAM system. The hollow boxes were printed using a nozzle diameter of 0.4 mm with constant printing parameters (Table 1) set by directly writing machine control commands (GCode), using in-house software to fully control the printing process (Allum et al., 2020), (Moetazedian et al., 2021a). The benefit of this approach compared to traditional slicer software with non-standardised print paths was previously validated (Allum et al., 2020), (Moetazedian et al., 2020a), (Moetazedian et al., 2021a). Specimens for tensile testing were designed at the scale of individual extruded filaments to allow precise characterisation of interfacial properties for comparison with bulk-material properties (Allum et al., 2020), (Moetazedian et al., 2020a). Specimens with a dog-bone geometry were achieved by modifying the extrusion volume along the toolpath to achieve wider extrusions in the specimen shoulder regions and narrower extrusions in the gauge regions (dimensions given in Fig. 1b and c). Specimens

Table 1
Printing parameters used to manufacture specimens with the RepRap ×400 system.

Printing parameters	Value
Nozzle temperature	210 °C
Print bed temperature	60 °C
Printing speed	1000 mm min^{-1}
Extruded-layer height	0.2 mm
Extruded-filament width in gauge	0.5 mm
Extruded-filament width in shoulders	0.75 mm

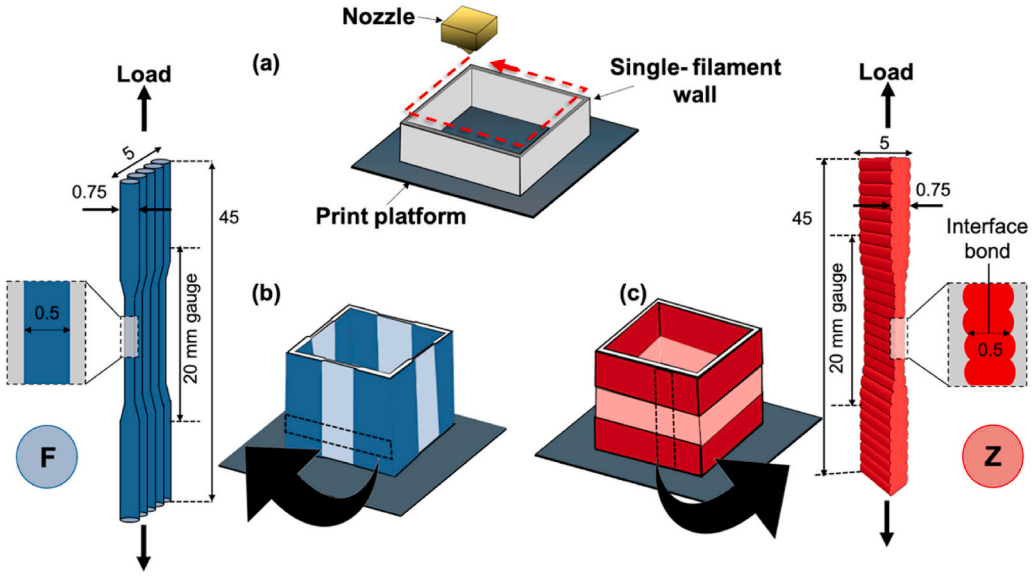

Fig. 1. (a) Explicit control of toolpath to generate single-filament walls for two testing directions: along extruded filament and parallel to print platform (b), and normal to the print platform (c). Arrows indicate the testing direction. Dashed rectangles on the boxes represent the outline of cut specimens. All dimensions are in mm.

successfully fractured within the gauge region. The overall dimensions were adapted from ASTM D1708 (D1708-18 and "Standard, 2002).

Damage accumulation was considered for 3D-printed PLA specimens when tested along extruded filaments (denoted as 'F'; representing bulk properties) and normal to extruded filaments (denoted as 'Z'; representing interfacial properties) as shown schematically in Fig. 1b and c, respectively. Each printed box was cut into 5-mm wide specimens using custom-developed tools and razor blades according to the method described elsewhere (Allum et al., 2020). No edge-effect upon the cutting process was noticed, since properties of specimens with variable widths (5 mm and 15 mm) were compared against those of injection-moulded PLA and no substantial difference was found (Moetazedian et al., 2020a).

2.2. Testing environments

Tensile-testing specimens (number of specimens n = 4) were used either as-printed (dry) or hydrated for 48 h in 30 ml of phosphate buffer saline (PBS) at physiological temperature (PT; 37 °C) to replicate in-vo conditions. To consider the effect of testing environment, tests were done under laboratory conditions (i.e. room temperature (RT) and humidity) and submerged in PBS at PT as shown in Fig. 2. Three main testing conditions were used in this study:

- S_{Ref} : dry specimens were tested under laboratory conditions in air at RT as the control group.
- S_H : hydrated specimens were tested under laboratory conditions in air at RT to investigate the effect of water absorption, which is typically used in literature to measure "wet properties".
- S_{PHS} : hydrated specimens were tested submerged at PT replicating in-vivo conditions to consider the combined effect of physiological temperature, hydration and submersion.

Acronyms were used in this study to refer to each specimen type with the naming method as follows: testing direction as superscript and testing environment as subscript. For example, to refer to dry Z specimens tested at RT, the acronym S^{Z}_{Ref} is used.

2.3. Characterisation

2.3.1. Water-absorption study

To check the water saturation of 3D-printed specimens (n = 3), both Z and F specimens were weighed immediately after the cutting process (W_0), using an analytical balance with an accuracy of ±0.0001 g. Specimens were stored in PBS at PT in an oven at 37 °C for 0.5 h, 12 h, 24 h and 48 h. At each respective time point, F and Z specimens were removed from the oven and excess moisture was removed using a paper towel prior to measuring the hydrated weight (W_H). The mean water absorption percentage was calculated using Equation (1).

$$Mean\ water\ absorption = \frac{W_H - W_0}{W_0} \times 100 \quad (1)$$

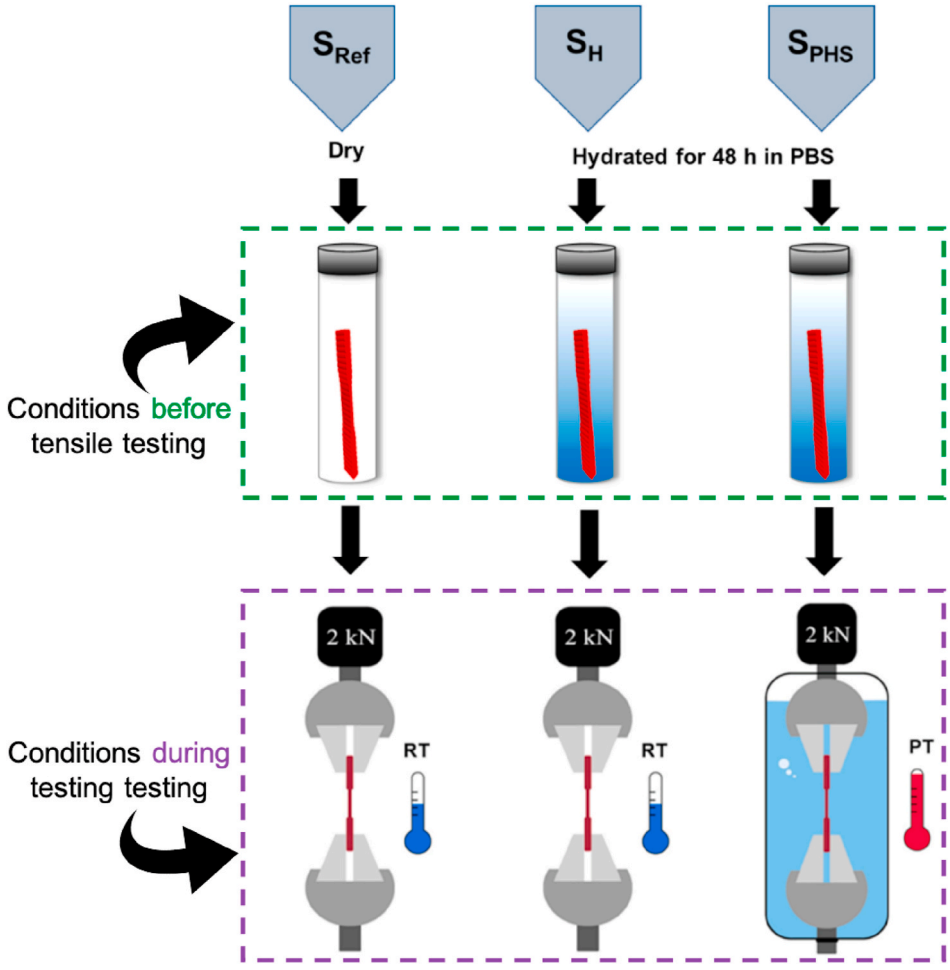

Fig. 2. Testing environments used for cyclic loading of 3D-printed PLA in this study: dry specimens were tested in air at RT (S_{Ref}) as the control group; hydrated specimens were either tested in air at RT (S_H) or submerged at PT (S_{PHS}).

2.3.2. Cyclic tensile testing

F and Z specimens (n = 4) were subjected to two cyclic loading conditions: (i) incremental amplitude (starting at 5 % of ultimate tensile strength (UTS), with increasing increments of 10 % of UTS from the second cycle until failure); (ii) constant amplitude (20 cycles at 70 % of UTS) to capture damage and mechanical properties close to the yield point. The amplitude steps were selected based on results from non-cyclic tension tests for each testing environment and direction. The number of cycles was chosen as 20 because stabilisation in energy dissipation was achieved within 20 cycles (the difference for mean energy dissipation between 10th and 20th cycle < 8 %). All tensile tests were performed at a strain rate of $4.0 \times 10^4\ s^{-1}$ (displacement of 0.5 mm min^{-1}), using a universal mechanical testing machine (Instron 5944, USA) equipped with a temperature-controlled bath (Instron Bio-Plus, Instron, USA) and a 1 kN load cell. A tensile test without a specimen loaded in the grips was carried out to confirm force measurements of resistance due to water were negligibly low (<2 % UTS). The levels of energy dissipation were calculated from the hysteresis of loading-unloading curves. For submerged testing, specimens were placed in the bath for 30 min prior to the start of the test to achieve uniform temperature and water absorption (Moetazedian et al., 2020a). Damage is frequently defined as the deterioration of elastic modulus, which was found to occur in the constant-amplitude tests. Thus, damage induced was calculated using a traditional notion of continuum damage mechanics (Lemaitre, 1996), (Abdo et al., 2019), (Moetazedian et al., 2020b):

$$D = 1 - \frac{E_D}{E_0} \tag{2}$$

where E_D is the residual modulus of the damaged material and E_0 is the modulus of the undamaged material.

For strength calculation, the pre-fracture area was measured using a Zeiss Primotech optical microscope at 5× magnification. For F specimens, the total cross-sectional area of extruded filaments was measured. For Z specimens, the average bond width was calculated based on 10 measurements for each specimen type (Moetazedian et al., 2020a), (Moetazedian et al., 2020b). In contrast to using caliper measurements (of overall extrusion width), this methodology allowed the actual load-bearing area to be considered to avoid miscalculation of bond strength. The mean mechanical properties for Z and F specimens were calculated from four replicates.

2.4. Statistical analysis

Statistical analysis was undertaken with Analysis ToolPak in Excel (2016), including one-way analysis of variance (ANOVA) and subsequent *t*-test using significant levels of $p \leq 0.05$.

3. Results and discussion

In this section, after initial confirmation of water saturation (Section 3.1) and comparison of stress-strain curves for non-cyclic and cyclic testing (Section 3.2), mechanical properties are evaluated in terms of constant-amplitude cyclic loading (Section 3.3), incremental-amplitude cyclic loading (Section 3.4) and damage of the unloading modulus (Section 3.5).

3.1. Water absorption

Saturation of the studied polymer prior to mechanical testing was measured to ensure that the effect of hydration was accurately considered. The result in Fig. 3 shows the evolution of water absorption for F and Z specimens up to 48 h. There was no significant difference between them ($p = 0.465$). Saturation of absorption in PLA happened within the first 30 min of hydration (water absorption 0.751 % ± 0.038) and stayed unchanged after 48 h (0.742 % ± 0.036). The obtained values agreed well with literature data reported for 3D-printed PLA (Moetazedian et al., 2020a), (Kakanuru and Pochiraju, 2020). For cyclic loading conditions, 48 h of hydration was sufficient to consider the effect of hydration.

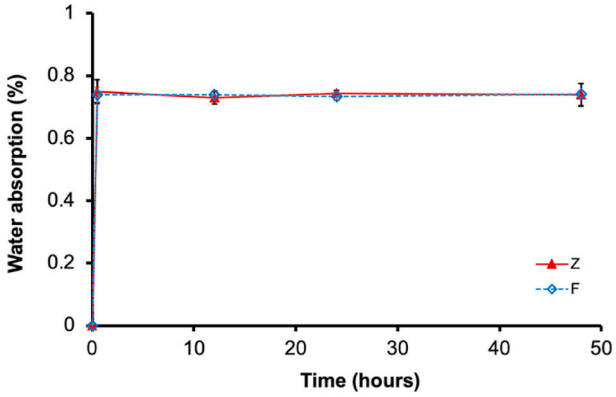

Fig. 3. Evolution of mean water absorption for F specimens (bulk PLA) and Z specimens (interface bond) stored at PT for up to 48 h. Error bars indicate standard deviation for the average values. No significant difference between F and Z was found.

3.2. Cyclic vs. non-cyclic loading

Typical stress-strain curves for F specimens (representing bulk material - Fig. 4a, c and e) and Z specimens (representing the interfacial bond - Fig. 4b, d and f) tested at cyclic (incrementally increasing) and non-cyclic loading conditions and different testing environments are shown in Fig. 4. UTS was similar for F and Z specimens but strain at failure was considerably different due to presence of naturally-occurring grooves (often considered as surface roughness) between layers in Z specimens. Apparently, the material was sufficiently ductile for stress concentration at these grooves not to affect UTS, but the associated strain localisation did affect strain at failure across the interface bond and led to brittle fracture, as discussed in recent studies (Allum et al., 2020), (Moetazedian et al., 2020a), (Moetazedian et al., 2021b).

The results can be considered with respect to (i) dependency of properties on testing environment and (ii) dependency of properties to cyclic/non-cyclic loading conditions. For the former, implementation of tests under conditions close to in-vivo (i.e. S_{PHS}) resulted in 47.6 % and 50.1 % reduction in UTS for F and Z specimens, respectively compared to S_{Ref}. The strain at failure was significantly increased by 32.3 relative percent (S_{PHS} relative to S_{Ref}) for Z, while, F specimens did not fail at 40% strain due to plasticising effects of water and temperature (Moetazedian et al., 2020a). For the typical testing environment used to measure 'wet properties' in many studies (i.e. S_H), the reduction in UTS compared to S_{Ref} was only 19.8 %, highlighting the importance of testing specimens at physiological temperature and submerged conditions - not only hydrated.

The incremental loading-unloading of 3D-printed PLA had a minimal detrimental effect on the mechanical properties: even for worst case scenario (i.e. the specimen with the greatest reduction in UTS; S^Z_{Ref}), 94.4 % of UTS of the standard test was still achieved. These results for incremental loading (Fig. 4) confirmed the suitability of 3D-printed PLA for biomedical applications with cyclic loading, since the difference in UTS for cyclic and non-cyclic loading, not reported previously, was less than approximately 10 % in all cases.

3.3. Constant-amplitude cyclic loading

The stress-strain curves for F and Z specimens subjected to constant-amplitude cyclic loading (70 % of UTS for 20 loading cycles - Fig. 5)

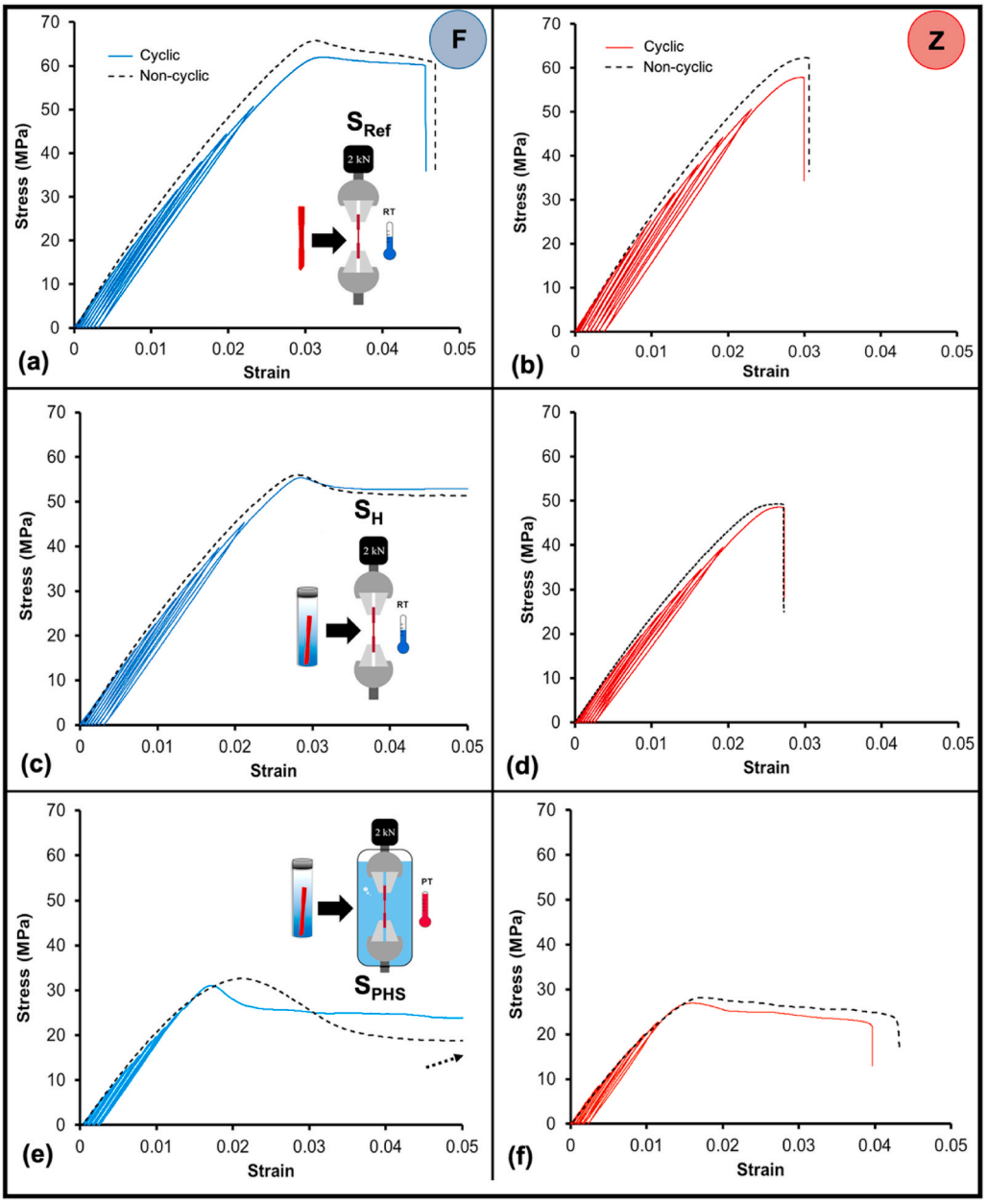

Fig. 4. Stress-strain curves for F specimens (a, c, e) and Z specimens (b, d, f) tested under non-cyclic (dashed line) and cyclic (solid line) conditions in different testing environments (a and b: S_{Ref}; c and d: S_H and e and f: S_{PHS}). The dotted arrow for S^F_{PHS} indicates no failure up to 40 % strain.

showed that for all specimen types and testing conditions, there was a large change from cycle 1 to 2, but changes in subsequent cycles were not significant, suggesting most of the inelastic behaviour happened within the first cycle.

To quantitatively compare the specimen types, two important aspects of loading-unloading curves were considered: (i) unloading modulus during each loading cycle (Fig. 6a and b); and (ii) residual strain after each loading cycle (Fig. 6e and f). For a direct comparison, all data were normalised by the respective value for the 1st cycle of each specimen type.

Results for the normalised unloading modulus (Fig. 6a and b) can be useful to understand the cyclic process by excluding some nonlinear aspects of the loading curve. Z specimens (Fig. 6b) showed a similar magnitude of reduction (within 5 %) in unloading modulus with increasing cycles to that of bulk PLA (i.e. F specimens), except for S_{PHS}. The difference in unloading modulus between the first and last cycles was not significant ($p > 0.05$ for S^F_{Ref}, S^Z_{Ref}, S^F_H and S^Z_H): 3.05 %, 3.07 %, 2.99 % and 2.81 % for S^F_{Ref}, S^Z_{Ref}, S^F_H and S^Z_H, respectively. For the environment close to in-vivo (S_{PHS}), the difference between the first and last cycle - F: 7.10 % and Z: 14.5 % - was significant ($p = 4.47 \times 10^{-4}$ for F and $p = 4.19 \times 10^{-3}$ for Z), possibly due to the plasticising effect of water and temperature, with a greater reduction in unloading modulus for Z specimens. The unloading modulus was still lower than the respective values for undamaged specimens, which was an indication of cyclic softening behaviour (Gong et al., 2017).

The levels of energy loss calculated from the loading-unloading curves for each cycle for F (Fig. 6c) and Z (Fig. 6d) specimens were similar (difference between F and Z specimens < 5 %). These results support our earlier findings that the interface between additive-manufactured layers had bulk strength under non-cyclic loading (Allum et al., 2020), (Moetazedian et al., 2020a). The interface (Z specimens) demonstrated similar degradation of properties to bulk polymer (F specimens) when tested under cyclic loading. This disagrees with the previous study by Afrose et al. (2016), who found that the

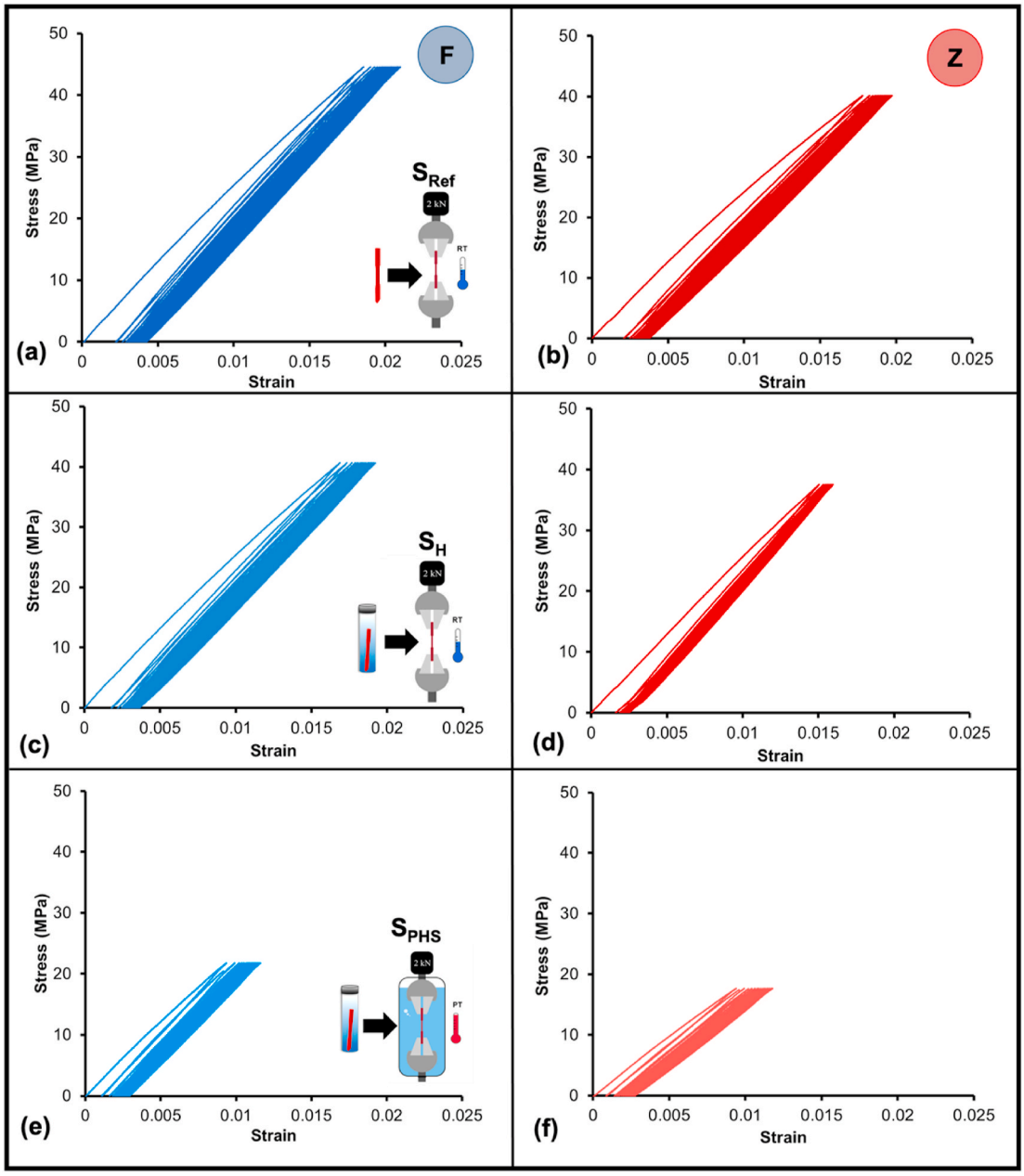

Fig. 5. Stress-strain curves for F specimens (a, c, e) and Z specimens (b, d, f) subjected to constant loading amplitude for 20 cycles with different testing environments (a and b: S_{Ref}; c and d: S_H and e and f: S_{PHS}). Most of the inelastic deformation occurred within the first cycle regardless of testing direction and environments.

interface bond had inferior properties to other build orientations during fatigue testing. However, Afrose et al. used ASTM standards for testing design, which we have previously argued (Allum et al., 2020) to limit the potential for fundamental characterisation, including challenges of measuring the contact area between layers.

The maximum energy dissipation was observed in the first cycle regardless of testing direction and environment. A similar trend was found for evolution of inelastic-strain, with such deformation occurring mostly in the first loading cycle. For both properties, after the first cycle there was a gradual decrease in values as the number of cycles increased until values stabilised after the 10th cycle. After this, the energy loss may be considered to be predominantly associated with viscous energy dissipation since it no longer relied on inelastic contributions. Although no considerable difference was found between F and Z specimens, the levels of energy dissipation and residual strain were dependent on the testing environment, as was also the case for unloading-modulus data. There was a significant decrease in energy loss between the 1st and 2nd cycles ($p < 0.05$ in all cases): 58.7 %, 61.0 %, 55.6 % and 61.3 % for S^F_{Ref}, S^Z_{Ref}, S^F_H and S^Z_H, respectively. This drop was lower but still significant for S_{PHS} specimens (48.4 % for Z ($p = 0.0328$) and 46.6 % for F ($p = 0.002$)). Higher energy dissipation for S_{PHS} in the 2nd cycle resulted in significantly higher residual strain in the 2nd cycle compared to other testing environments (Fig. 6e and f) – $p < 0.05$ between S_{PHS} and S_{Ref}/S_H. This could be explained by the effect of water molecules and temperature to enhance the viscosity of the material. The evolution of energy loss and residual strain were dependent on the testing environment since S_{PHS} showed higher normalised values of energy dissipation and residual strain than S_{Ref}/S_H ($p < 0.05$ in all cases except for energy dissipation values for F specimens), confirming changes in the polymers behaviour when tested under conditions close to in-vivo.

To understand and assess the contribution of viscoelastic behaviour of the material to the damage accumulation during cyclic loading,

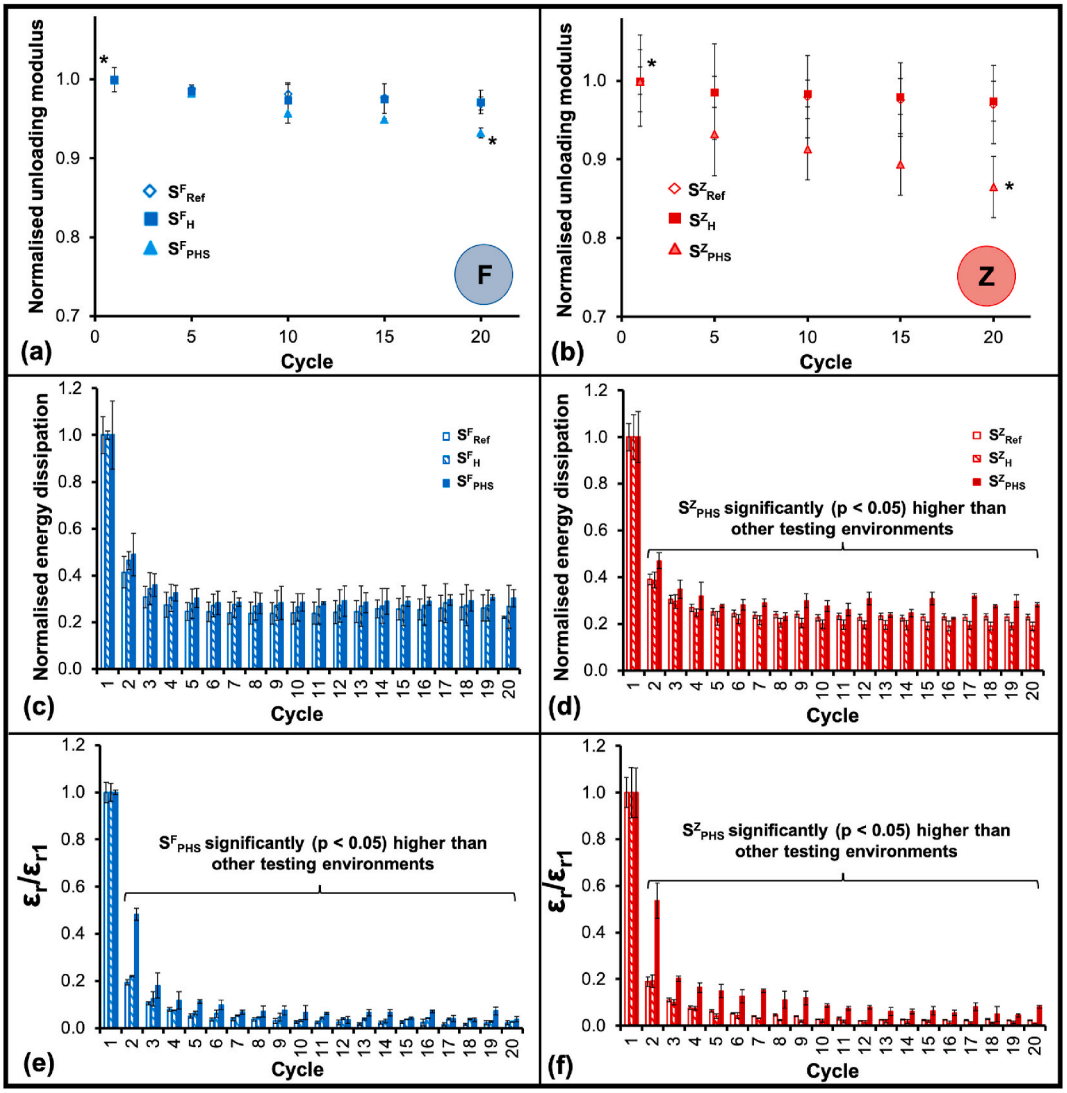

Fig. 6. Evolution of normalised unloading modulus (a and b), energy dissipation (c and d) and residual strain (e and f) for F specimens (a, c, e) and Z specimens (b, d, f) tested under different testing environments. S_{PHS} showed higher values compared to others. Whilst there was no difference between F and Z specimens. Error bars indicate standard deviation. (*$p < 0.05$ for comparison of the first and last cycle for S_{PHS} in a and b).

additional creep tests were performed. Z specimens were subjected to 60 % of UTS for a period of 1010 s (equal to the total duration of 20 cycles in the cyclic testing) under S_{Ref} and S_{PHS} conditions. At the end of the test, the specimens were unloaded to determine the extent of damage by calculating the degradation of the elastic modulus. The obtained normalised creep strain curves (normalised by the applied strain at 60 % UTS) for specimens under these two conditions ($n = 2$ for each condition) are shown in Fig. 7a, along with the normalised modulus (for both loading and unloading) in Fig. 7b. The extent of damage reflected in the decline in the elastic modulus after the creep test (<2 % reduction) was lower than that found in cyclic testing (from 2.81 % to up to 14.5 % – see Fig. 6a and b). Therefore, the contribution of damage was negligible, and most of the strain accumulation in cyclic loading was due to viscous behaviour of the material.

Stress relaxation was also studied for Z specimens tested under S_{PHS} conditions ($n = 2$) by loading up to 60 % of UTS and maintaining the associated strain (0.0070 for S_{PHS}) for the same time of 1010 s. Whilst the strain level was kept constant, a continuous relaxation of stress was exhibited by the specimens (Fig. 7c). In contrast, Z specimens tested in S_{Ref} conditions demonstrated no stress relaxation, emphasizing the importance of testing in physiological conditions.

The residual strain values normalised by the magnitude after the 10th cycle were also plotted for both F (Fig. 8a) and Z (Fig. 8b) specimens, and no considerable variation between testing directions was apparent. In all cases, the accumulation of strain with an increasing number of cycles was observed, referred to as "*ratchetting*" and commonly found in metals (Kang and Liu, 2008), (Kang and Ratchetting, 2008). Although F and Z specimens behaved similarly, S_{Ref} and S_H demonstrated more of a plateau in residual-strain accumulation compared to S_{PHS}. To quantify this, a parameter (α) was used as a ratio of difference between the 20th and 10th cycles and the value for the 10th cycle. The calculated values are summarised in Table 2 and demonstrate a dependency on the testing environment; α approximately doubled for S_{PHS} compared to that of S_{Ref} since the viscosity of the material was enhanced. In addition, changes in residual strain for each cycle ($\Delta\varepsilon_r$) were calculated for two consecutive cycles (Fig. 8c and d). The evolution of incremental residual strain can be divided into two stages: (i) initial large inelastic deformation and (ii) its saturation, with predominantly viscoelastic material responses for each cycle.

The degradation of mechanical properties due to cyclic loading was similar for the interface between additive-manufacturing layers (Z specimens) and the bulk material (F specimens). It appeared that evolution of certain properties such as energy dissipation and residual strain were considerably influenced by the testing environments and future

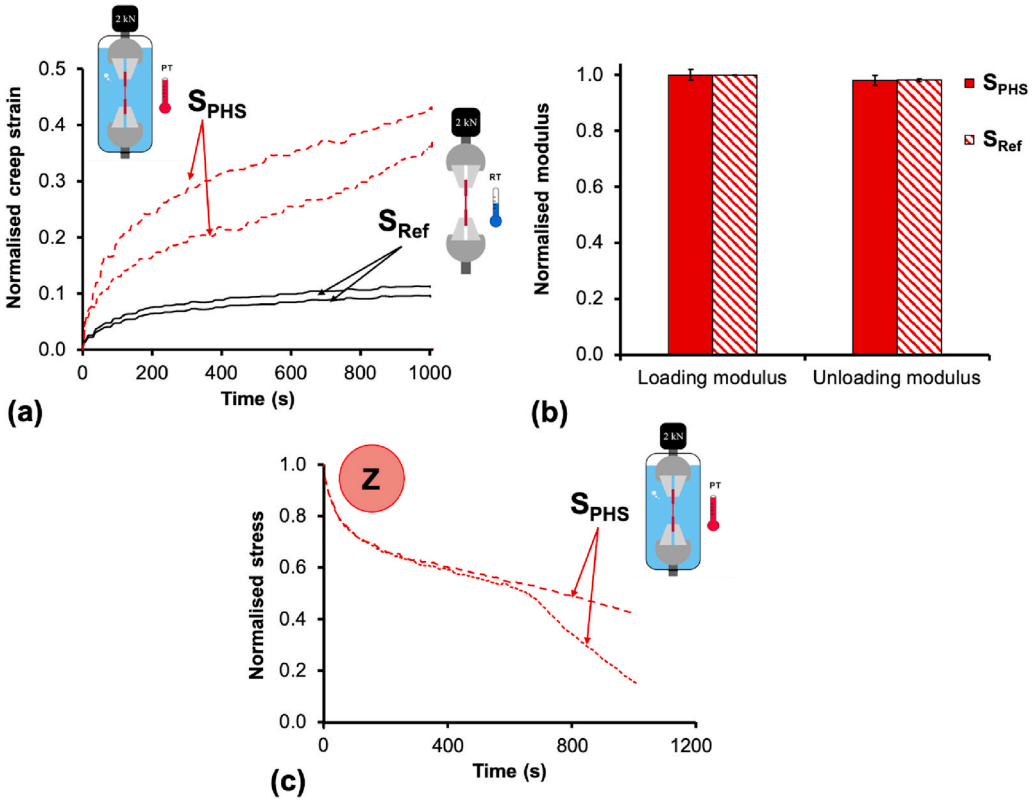

Fig. 7. Creep and relaxation behaviour of Z specimens. (a) Normalised creep strain during static creep testing under loading of 60 % UTS for S^{Z}_{Ref} and S^{Z}_{PHS}. (b) Loading and unloading modulus before and after creep testing indicated minimal deterioration of modulus (<2 % change). (c) Stress relaxation curves for S^{Z}_{PHS}. Error bars indicate standard deviation.

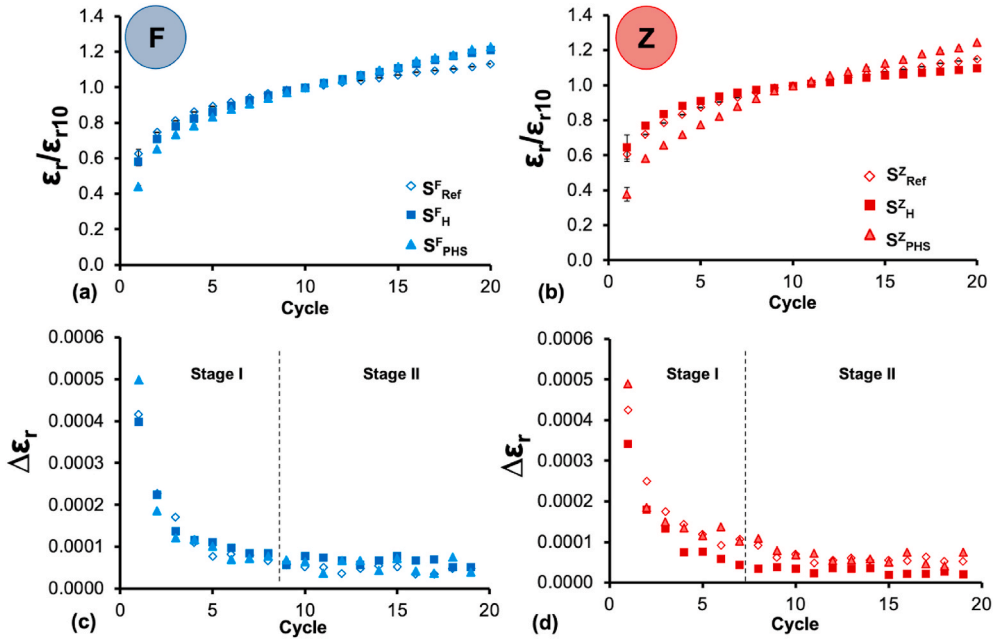

Fig. 8. Evolution of normalised residual strain evolution for F specimens (a) and Z specimens (b) tested at different testing environments. (c) and (d) incremental changes in residual strain at different testing environments showed two stages in deformation of material during cyclic loading: (i) initial large inelastic deformation and (ii) viscoelastic response of material after saturation of inelastic deformation. Error bars indicate standard deviation.

studies for biomedical applications are advised to test polymers under conditions close to the in-vivo environment.

3.4. Varying-amplitude cyclic loading

Cyclic loading with an incrementally increasing amplitude was undertaken for F (Fig. 9a and c) and Z (Fig. 9b and d) specimens. Data for

Table 2
Parameter α for F and Z specimens tested in different environments.

Parameter α					
S^F_{Ref}	S^Z_{Ref}	S^F_H	S^Z_H	S^F_{PHS}	S^Z_{PHS}
0.13	0.15	0.20	0.11	0.23	0.25

strain and energy dissipation were normalised by the magnitude of the 5th cycle to allow direct comparison. Similar to constant-amplitude cyclic loading in Section 3.3, there was no substantial differences between F and Z specimens when tested under incremental loading amplitudes. For all specimen types, residual strain was present from the second cycle, suggesting that material yielding happened at a similar fraction of UTS in all testing environments. With increasing stress levels, residual strain and energy loss showed a nearly linear increase for the entire process (after a brief initial delay), with comparable energy dissipation values for S_{PHS} and S_{Ref} ($p > 0.05$ for both F and Z specimens) regardless of testing direction. In the 9th cycle (80 % of UTS), the energy dissipation for S_{Ref} was approximately 24 % more than for S_{PHS} ($p = 0.0155$ between S^F_{Ref} and S^F_{PHS} and $p = 0.023$ between S^Z_{Ref} and S^Z_{PHS}). Specimens tested in air at RT (i.e. S_{Ref}) failed abruptly in the next cycle, while, S_{PHS} showed more deformation than S_{Ref} before failure.

The evolution of unloading modulus for incremental loading amplitude (Fig. 10) showed cyclic softening behaviour similar to the constant-amplitude results (Fig. 6). However, for reference testing conditions (S_{Ref}), the magnitude of reduction in unloading modulus from the 1st to 9th cycle was significant ($p < 0.05$), and it was quintupled for incremental amplitude (10.3 % and 10.1 % for S^F_{Ref} and S^Z_{Ref}, respectively) compared to loading with a constant amplitude (1.7 % and 2.3 % for S^F_{Ref} and S^Z_{Ref}, respectively). These results are further evidence that most damage in terms of deterioration of the modulus occurred when the material was loaded beyond 70 % of UTS. In contrast, for S_{PHS}, similar magnitudes of reduction for incremental-amplitude tests (S^F_{PHS}: 9.3 % and S^Z_{PHS}: 12.3 %) and constant-amplitude tests (5.8 % and 10.9 % for S^F_{Ref} and S^Z_{Ref}, respectively) were obtained, again highlighting the importance of considering the testing environment.

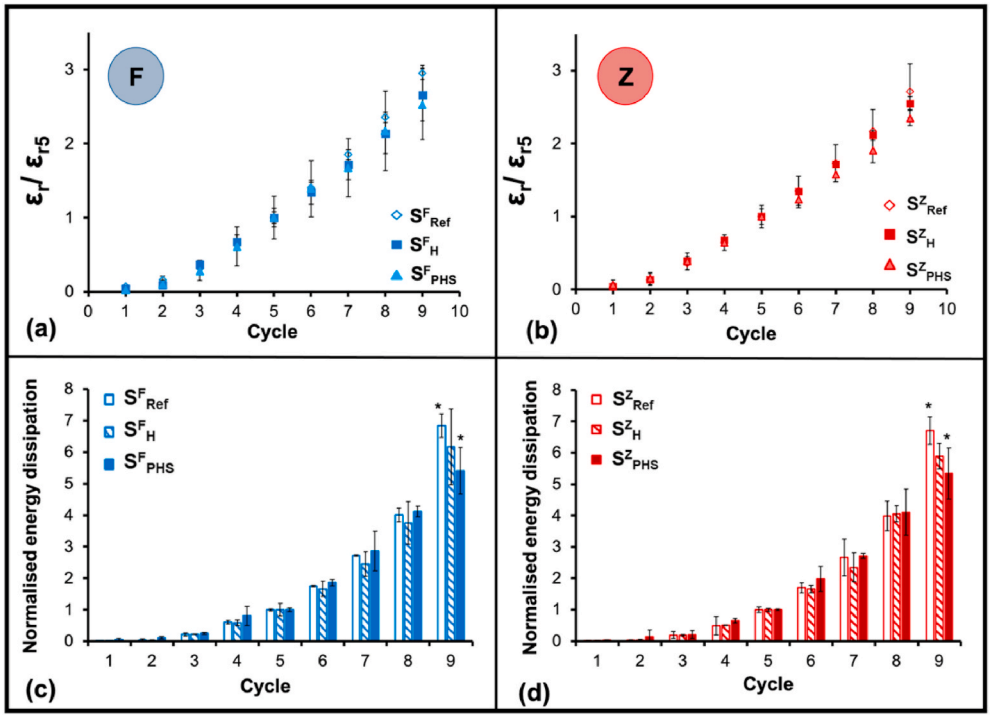

Fig. 9. Evolution of normalised residual strain and energy dissipation for F specimens (a and c) and Z specimens (b and d) when tested in different testing environments. The majority of damage did not happen until the later stages of cyclic loading. Error bars indicate standard deviation. (* above bar charts in c and d indicate $p < 0.05$ between S_{Ref} and S_{PHS}).

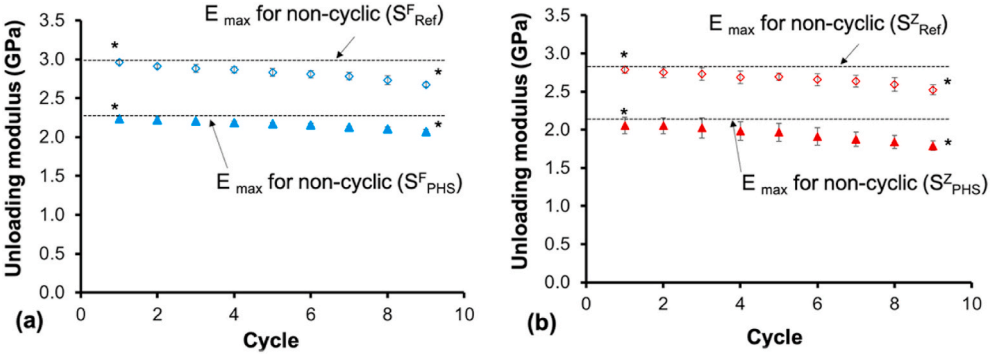

Fig. 10. Unloading modulus for F specimens (a) Z specimens (b) when tested at S_{Ref} and S_{PHS} conditions under incremental amplitude. Error bars indicate standard deviation. (*$p < 0.05$ between the 1st and 9th cycle).

The relationships between accumulated energy dissipation and residual strain for both constant- and incremental-amplitude conditions are given in Fig. 11. The results showed an exponential growth in all cases; the increase in accumulated energy happened at later stages of cyclic loading, supporting our earlier findings. There was a limit for residual strain as it approached a value of 0.004. The zoomed-in inset plots indicate that below strains of 0.0015, which coincided with 7th cycle (70 % of UTS), the accumulated energy was very low, while beyond that point, there was a sharp increase. These graphs can be useful for design of new medical implants, serving as a guide to understand reasonable strain limits and damage accumulation for 3D-printed PLA.

3.5. Damage evolution based on modulus degradation

The analysis was conducted to assess the sensitivity of damage behaviour with reference to its initiation and growth for different testing directions (F and Z) and environments (S_{Ref}, S_H and S_{PHS}). The damage (linked to the extent of module degradation) for each cycle of incremental loading is plotted as a function of normalised strain (strain/strain at maximum force) in Fig. 12. For simplicity, only the average values for S_{Ref} and S_{PHS} are shown. The character of damage evolution for all specimen types was relatively similar. A slightly higher damage accumulation was observed in Z specimens than F specimens. The data suggest that accumulation of damage is not highly dependent on the testing environment but is primarily a function of normalised strain.

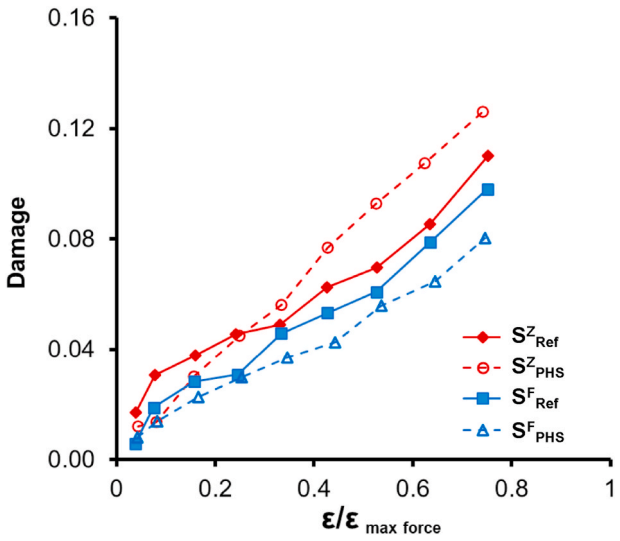

Fig. 12. Damage evolution based on degradation of unloading modulus for incremental-amplitude tests showed almost a linear trend for all cases.

4. Conclusions and future work

The influence of the testing environment on cyclic-loading properties of additive-manufactured PLA specimens was studied. The obtained results showed that there was no significant difference between specimens tested along extruded filaments (F; representing bulk polymer material) and normal to the extruded filament (Z; representing the interfacial bond between additive-manufactured layers) under constant- and incremental-amplitude loading conditions for a given number of cycles. In addition, the difference in UTS between cyclic and non-cyclic loading conditions was less than approximately 10%, giving confidence

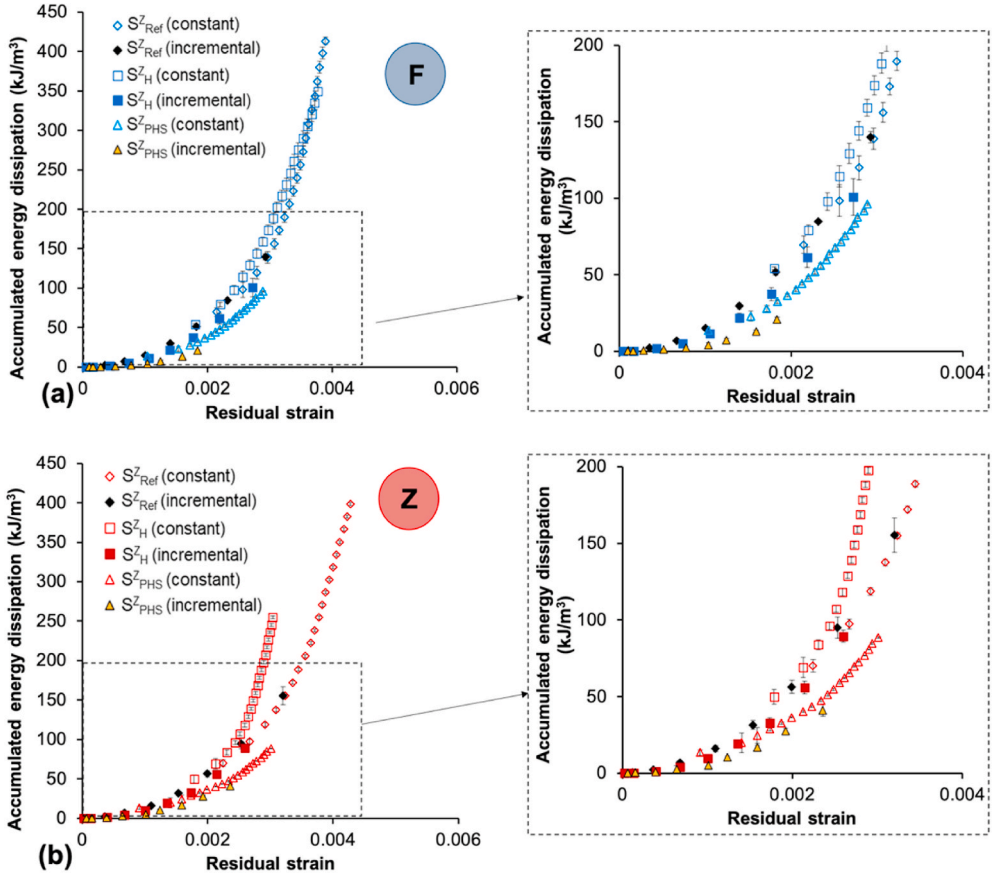

Fig. 11. Accumulated energy dissipation for F (a) and Z (b) specimens for constant- and incremental-loading amplitude tests for different testing environments. Zoomed-in insets indicate that a rapid increase in energy dissipation happened beyond residual strain of 0.0015. Error bars indicate standard deviation.

for the use of 3D-printed PLA in biomedical applications where repetitive loading is expected. For both cyclic testing conditions, PLA specimens showed cyclic softening behaviour. For cyclic tests with a constant loading amplitude, higher residual deformation (>100 % greater) and energy dissipation (>15 % greater) were found when testing under conditions close to in-vivo (submerged in water at physiological temperature) as opposed to laboratory conditions (in air at room temperature). This difference may be due to plasticisation effects of water and temperature. Ratchetting strain accumulation (continuously increasing residual strain with each cycle) was identified for all specimen types during cyclic loading. For cyclic tests with incrementally increasing loading amplitude, most of the energy dissipation occurred in the last two cycles before failure, when the polymer approached the yield point. Estimation of damage initiation and its growth showed a linear trend regardless of testing environment suggesting that damage was predominantly a function of stress.

Investigating the mechanical behaviour of 3D printed PLA at lower stress levels for a high number of cycles would be interesting, since the specimen design developed for tensile testing would allow precise characterisation of fatigue properties of the interlayer bond. Additionally, considering using the current tensile-testing design (i.e. single filament specimens) to measure and analyse the damage evolution for other 3D-printable polymers would be beneficial for development of AM parts for biomedical application.

CRediT authorship contribution statement

Amirpasha Moetazedian: Investigation, Data curation, Conceptualization, Methodology, Formal analysis, Writing – original draft, Visualization. **Andrew Gleadall:** Conceptualization, Methodology, Formal analysis, Writing – review & editing. **Elisa Mele:** Conceptualization, Methodology, Formal analysis, Writing – review & editing. **Vadim V. Silberschmidt:** Conceptualization, Methodology, Formal analysis, Writing – review & editing.

Declaration of competing interest

The authors declare that they have no known competing financial interests or personal relationships that could have appeared to influence the work reported in this paper.

References

Abbott, A.C., Tandon, G.P., Bradford, R.L., Koerner, H., Baur, J.W., 2018. Process-structure-property effects on ABS bond strength in fused filament fabrication. Addit. Manuf. vol. 19, 29–38.

Abdo, D., Gleadall, A., Silberschmidt, V.V., 2019. Damage and damping of short-glass-fibre-reinforced PBT composites under dynamic conditions: effect of matrix behaviour. Compos. Struct. vol. 226, 11286.

Afrose, M.F., Masood, S.H., Iovenitti, P., Nikzad, M., Sbarski, I., 2016. Effects of part build orientations on fatigue behaviour of FDM-processed PLA material. Prog. Addit. Manuf. vol. 1 (1), 21–28.

Aliheidari, N., Christ, J., Tripuraneni, R., Nadimpalli, S., Ameli, A., 2018. Interlayer adhesion and fracture resistance of polymers printed through melt extrusion additive manufacturing process. Mater. Des. vol. 156, 351–361.

Allum, J., Moetazedian, A., Gleadall, A., Silberschmidt, V.V., Aug. 2020. Interlayer bonding has bulk-material strength in extrusion additive manufacturing: new understanding of anisotropy. Addit. Manuf. vol. 34, 101297.

Bachtiar, E.O., et al., 2020. 3D printing and characterization of a soft and biostable elastomer with high flexibility and strength for biomedical applications. J. Mech. Behav. Biomed. Mater. vol. 104, 103649.

Bellehumeur, C., Li, L., 2004. Modeling of bond formation between polymer filaments in the fused deposition modeling process. J. Manuf. Process. vol. 6 (2), 170–178.

Christiyan, K.G.J., Chandrasekhar, U., Venkateswarlu, K., 2016. A study on the influence of process parameters on the mechanical properties of 3D printed ABS composite. IOP Conf. Ser. Mater. Sci. Eng. vol. 114, 12109.

Coogan, T.J., Kazmer, D.O., 2017a. Bond and part strength in fused deposition modeling. Rapid Prototyp. J. vol. 23 (2), 414–422.

Coogan, T.J., Kazmer, D.O., 2017b. Healing simulation for bond strength prediction of FDM. Rapid Prototyp. J. vol. 23 (3), 551–561.

ASTM D1708-18, 2002. Standard Test Method for Tensile Properties of Plastics by Use of Microtensile.

Da Silva, D., et al., 2018. Biocompatibility, biodegradation and excretion of polylactic acid (PLA) in medical implants and theranostic systems. Chem. Eng. J. vol. 340, 9–14.

Elsawy, M.A., Kim, K.H., Park, J.W., Deep, A., 2017. Hydrolytic degradation of polylactic acid (PLA) and its composites. Renew. Sustain. Energy Rev. vol. 79, 1346–1352.

Farah, S., Anderson, D.G., Langer, R., 2016. "Physical and mechanical properties of PLA, and their functions in widespread applications — a comprehensive review. Adv. Drug Deliv. Rev. vol. 107, 367–392.

Gleadall, A., Visscher, D., Yang, J., Thomas, D., Segal, J., 2018a. "Review of additive manufactured tissue engineering scaffolds: relationship between geometry and performance," *Burn.* Trauma vol. 6, 1–16.

Gleadall, A., Poon, W., Allum, J., Ekinci, A., Han, X., Silberschmidt, V.V., 2018b. Interfacial fracture of 3D-printed bioresorbable polymers. Procedia Struct. Integr. vol. 13, 625–630.

Gong, B., Cui, S., Zhao, Y., Sun, Y., Ding, Q., 2017. Strain-controlled fatigue behaviors of porous PLA- based scaffolds by 3D-printing technology. J. Biomater. Sci. Polym. Ed. vol. 5063, 1–9.

Kakanuru, P., Pochiraju, K., 2020. Moisture ingress and degradation of additively manufactured PLA, ABS and PLA/SiC composite parts. Addit. Manuf., 101529 (in press).

Kang, G., Liu, Y., 2008. Uniaxial ratchetting and low-cycle fatigue failure of the steel with cyclic stabilizing or softening feature. Mater. Sci. Eng. vol. 472 (1–2), 258–268.

Kang, G., 2008. Ratchetting: Recent progresses in phenomenon observation, constitutive modeling and application. Int. J. Fatig. vol. 30 (8), 1448–1472.

Lawrence, S. St, Willett, J.L., Carriere, C.J., 2001. Effect of moisture on the tensile properties of poly(hydroxy ester ether). Polymer vol. 42 (13), 5643–5650.

Lemaitre, J., 1996. A Course on Damage Mechanics. Springer.

Ligon, S.C., Liska, R., Stampfl, J., Gurr, M., Mülhaupt, R., 2017. Polymers for 3D printing and customized additive manufacturing. Chem. Rev. vol. 117 (15), 10212–10290.

Moetazedian, A., Gleadall, A., Han, X., Silberschmidt, V.V., 2020a. Effect of environment on mechanical properties of 3D printed polylactide for biomedical applications. J. Mech. Behav. Biomed. Mater. vol. 102, 103510.

Moetazedian, A., Gleadall, A., Mele, E., V Silberschmidt, V., 2020b. "Damage in extrusion additive manufactured parts : effect of environment and cyclic loading. Procedia Struct. Integr. vol. 28, 452–457.

Moetazedian, A., Budisuharto, A.S., Silberschmidt, V.V., Gleadall, A., 2021a. CONVEX (CONtinuously Varied EXtrusion): a new scale of design for additive manufacturing. Addit. Manuf. vol. 37, 101576.

Moetazedian, A., Gleadall, A., Han, X., Ekinci, A., Mele, E., Silberschmidt, V.V., 2021b. Mechanical performance of 3D printed polylactide during degradation. Addit. Manuf. vol. 38, 101764.

Nair, L.S., Laurencin, C.T., 2007. Biodegradable polymers as biomaterials. Prog. Polym. Sci. vol. 32 (8–9), 762–798.

Ning, F., Cong, W., Hu, Y., Wang, H., 2017. Additive manufacturing of carbon fiber-reinforced plastic composites using fused deposition modeling: effects of process parameters on tensile properties. J. Compos. Mater. vol. 51 (4), 451–462.

Pan, A., Huang, Z., Guo, R., Liu, J., 2015. Effect of FDM process on adhesive strength of polylactic acid(PLA) filament. Key Eng. Mater. vol. 667, 181–186.

Safai, L., Cuellar, J.S., Smit, G., Zadpoor, A.A., 2019. A review of the fatigue behavior of 3D printed polymers. Addit. Manuf. vol. 28, 87–97.

Senatov, F.S., V Niaza, K., Stepashkin, A.A., Kaloshkin, S.D., 2016. Low-cycle fatigue behavior of 3d-printed PLA-based porous scaffolds. Compos. Part B vol. 97, 193–200.

Spoerk, M., Arbeiter, F., Cajner, H., Sapkota, J., Holzer, C., 2017. Parametric optimization of intra- and inter-layer strengths in parts produced by extrusion-based additive manufacturing of poly(lactic acid). J. Appl. Polym. Sci. vol. 134 (41), 1–15.

Spoerk, M., Gonzalez-Gutierrez, J., Sapkota, J., Schuschnigg, S., Holzer, C., 2018. Effect of the printing bed temperature on the adhesion of parts produced by fused filament fabrication. Plast. Rubber Compos. vol. 47 (1), 17–24.

Wu, L., Zhang, J., Jing, D., Ding, J., 2006. "'Wet-state' mechanical properties of three-dimensional polyester porous scaffolds. J. Biomed. Mater. Res. vol. 76 (2), 264–271.

Xu, H., Yang, X., Xie, L., Hakkarainen, M., 2016. Conformational footprint in hydrolysis-induced nanofibrillation and crystallization of poly(lactic acid). Biomacromolecules vol. 17 (3), 985–995.